GLOMULINA OCULUS, NEW CALCAREOUS FORAMINIFERAL SPECIES FROM THE HIGH ARCTIC: A POTENTIAL INDICATOR OF A NEARBY MARINE-TERMINATING GLACIER

ANNE E. JENNINGS^{1,*}, MARIT-SOLVEIG SEIDENKRANTZ² AND KAREN LUISE KNUDSEN²

ABSTRACT

A new calcareous Arctic foraminiferal species, Glomulina oculus n. sp., belonging to the suborder Miliolina has been observed in surface samples from northern Nares Strait and Petermann Fjord, NW Greenland, and off Zachariae Isbrae, NE Greenland, as well as in early Holocene sediments from the northern Baffin Bay region and on the NE Greenland shelf. In some samples, this new porcelaneous species makes up a significant fraction of the foraminiferal assemblage, particularly in samples with a relatively large sand content, and we suggest that this species is indicative of an Arctic environment with marine-terminating glaciers. Yet, further studies are needed to ascertain its full habitat range.

INTRODUCTION

A new species of calcareous benthic foraminifera belonging to the suborder Miliolina was found in modern (including Rose Bengal stained specimens) and Holocene seafloor sediments from Petermann Fjord and northern Nares Strait in NW Greenland, in the northernmost Baffin Bay, and on the NE Greenland shelf. Despite it being a distinct and common species in these areas, careful searches of the literature and queries to other foraminiferal experts with experience in Arctic faunas did not yield any previous identification of this species. Therefore, we have concluded that the species, though common in certain Arctic environments, has not been described previously. The species is referred to the genus *Glomulina*, bringing the number of species in this genus to three (cf., Ellis & Messina, 2019) and we here name the species *Glomulina oculus*.

Glomulina oculus n. sp. was first noted in modern and Holocene seafloor sediments sampled during the 2015 Petermann Glacier Expedition to northern Nares Strait and the Petermann Fjord, NW Greenland. The species was noted routinely during shipboard scanning for foraminiferal content in sediment cores during visual core descriptions. Both living (Rose Bengal stained) and dead (unstained) specimens were observed in many of the multicore tops. Rare unstained Glomulina oculus specimens were furthermore observed in the Uwitec core tops from below the floating ice tongue. Subsequently, Glomulina oculus was also identified in early Holocene records from marine sediment cores in the northernmost Baffin Bay, near Smith Sound and in Lancaster

STUDY REGIONS Northern Nares Strait and Petermann Fjord

Sound. In addition, it has been found in both surface sediments (one Rumohr core top sample) and early Holocene

Herein we describe the new species and its modern envi-

ronmental preferences as well as the implications of its oc-

currences in paleoenvironmental reconstructions. We only

include the data relevant for the presentation of this new

species, while further investigations of the foraminiferal as-

glaciomarine sediments from the NE Greenland shelf.

The modern samples for this study were primarily acquired from the northern Nares Strait (northern Kennedy Channel, Hall Basin, southern Robeson Channel and the Petermann Fjord, including beneath the floating ice tongue; Fig. 1A, B). These high Arctic sites are situated above 80°N and are strongly influenced by both sea ice and terrestrial glacier ice, including plateau ice caps and the Petermann Glacier, a main outlet glacier of the Greenland ice sheet that terminates in a 47-km-long floating ice tongue (Münchow et al., 2016). The area is bathymetrically complex with many basins formed by underlying bedrock topography and molded by confluent ice streams during the last glaciation (Jakobsson et al., 2018).

The water column in the region is stratified with very cold, low salinity Polar Water from the Arctic Ocean forming the upper ~50 to 100 m, overlying relatively warm and saline (~0.3°C, 34.8 psu) Atlantic Water (Fig. 2). The Atlantic Water is derived from the Atlantic Layer in the Arctic Ocean, and it enters Nares Strait over a 290-m-deep sill in the Lincoln Sea (Münchow et al., 2011, 2016) before it passes over a 440-m-deep sill at the mouth of the Petermann Fjord to form the bottom water in the fjord (Münchow et al., 2016; Jakobsson et al., 2018; Fig. 1B). Rising glacier meltwater and Atlantic Water mix near the Petermann Glacier grounding line to form a transitional layer above the Atlantic Water (Münchow et al., 2016; Washam et al., 2019). Slight but significant warming of Atlantic Water has been observed in Nares Strait and the Petermann Fjord over the last decade (Münchow et al., 2011; Washam et al., 2018). The Petermann Glacier meltwater influx can be traced throughout Hall Basin but is relatively more concentrated along the Greenland side as it exits the fjord (Heuzé et al., 2017).

Land-fast sea ice covers the northern Nares Strait for most of the year, followed by a 3 to 4-month period of mobile pack ice. The sea-ice regime is governed by the formation of ice arches that form by consolidation of thick multi-year Arctic Ocean sea-ice floes that converge in the Lincoln Sea at the northern end of the strait (Kozo, 1991),

semblages in the Lancaster Sound and NE Greenland shelf study sites will be presented elsewhere.

 $^{^{\}rm 1}$ INSTAAR, University of Colorado, Boulder, Colorado 80309-0450 USA

² Paleoceanography and Paleoclimate Group, Department of Geoscience, Arctic Research Centre, and Climate Interdisciplinary Centre for Climate Change, Aarhus University, Høegh-Guldbergs Gade 2, 8000 Aarhus C, Denmark

^{*}Correspondence author. E-mail: anne.jennings@colorado.edu

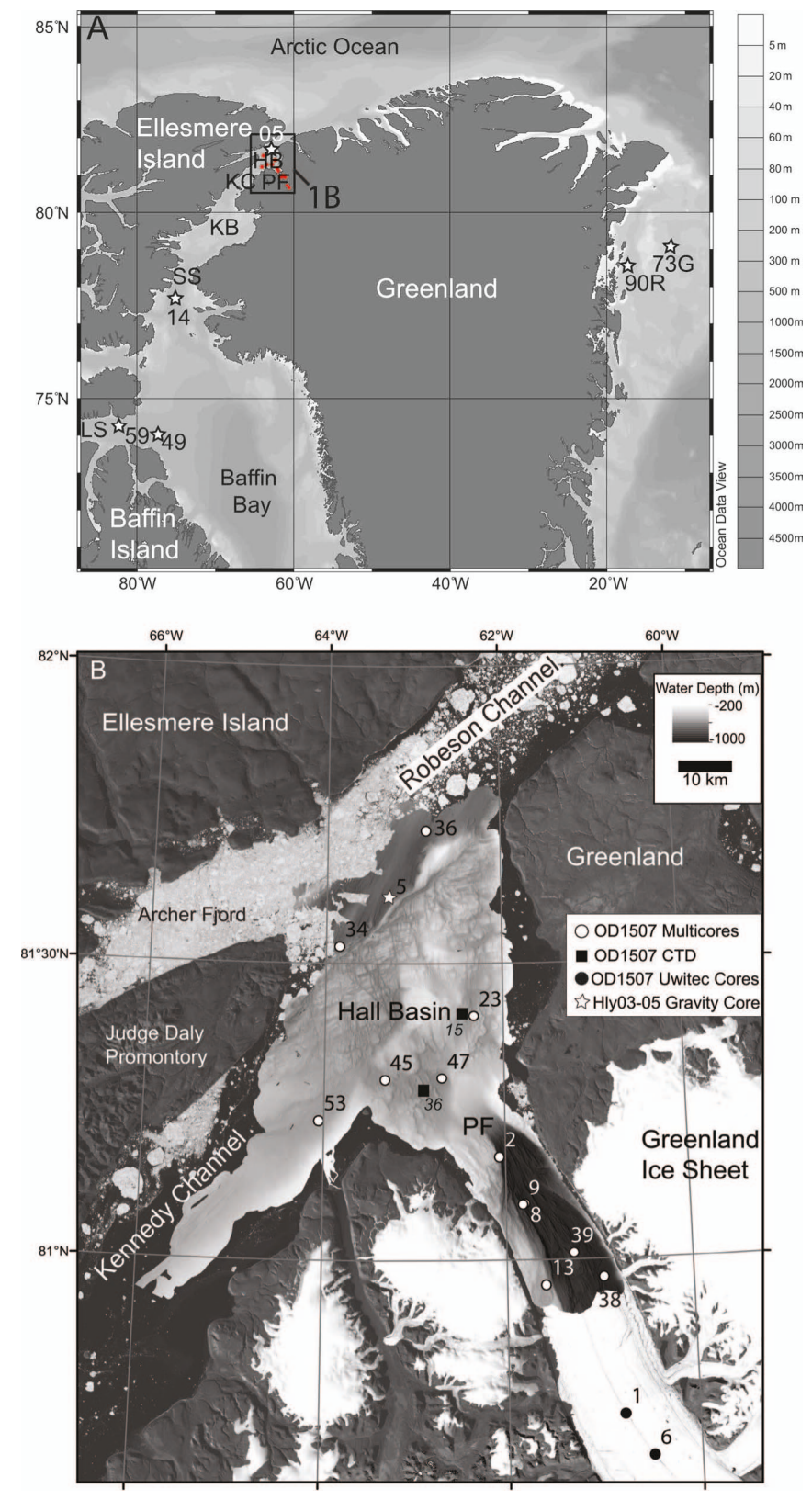


FIGURE 1. A Map depicting the cores (stars), where *Glomulina oculus* n. sp. has been found in early Holocene glaciomarine sediments in Hall Basin, northernmost Baffin Bay, Lancaster Sound, and on the NE Greenland shelf. SS = Smith Sound, LS = Lancaster Sound, PF = Petermann Fjord, HB = Hall Basin, KC = Kennedy Channel, KB = Kane Basin, 05 = core Hly03O5GC, 14 = piston core 2001LSSL-014PC, 49 = piston core 2008029-49PC, 59 = piston core 2008029-59PC, 73G = gravity core DA17-NG-ST07-73G, 90R = Rumohr core DA17-NG-ST08-90R. The box indicates the area shown in detail in Fig. 1B. B Detailed map of northern Nares Strait and Petermann Fjord showing locations of multicores (white circles) and Uwitec cores (black circles), where modern samples were taken. Specimens of *G. oculus* were found in all these surface sediment samples.

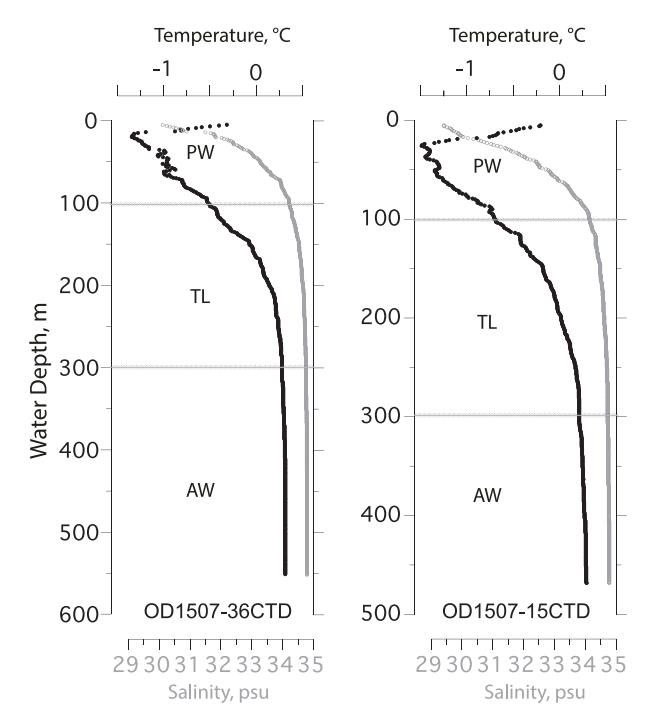


FIGURE 2. Conductivity-Temperature-Depth (CTD) profiles from OD1507-36CTD and -15CTD (Fig. 1B) the CTD casts nearest to sites OD1507-23MC and -47MC with the largest numbers of *Glomulina oculus*. Data from Muenchow (2019). PW = Polar Water, TL = Transitional Layer, <math>AW = Atlantic Water.

or more commonly in the Kane Basin at the southern end. Ice arches form in late fall and early winter and effectively block Arctic sea-ice flow through the Nares Strait (Kwok, 2005), while allowing Polar Water to flow beneath the sea ice. Break-up of the ice arches occurs sometime between mid-July to mid-August, resulting in mobilization of sea ice through Nares Strait toward Baffin Bay driven by strong northerly winds (Samelson et al., 2006). Sea-ice conditions in recent years are more variable as the formation of northern and southern ice arches become less reliable, resulting in some years with a longer or even continuous mobile sea-ice season (Kwok et al., 2010; Ryan & Münchow, 2017).

NORTHERN BAFFIN BAY

The northern Baffin Bay, including Lancaster Sound, sediment core sites (Fig. 1A), are influenced by cold, low salinity Polar Water from the surface of the Arctic Ocean that flows through both Lancaster Sound and Nares Strait forming the surface water in Baffin Bay (Tang et al., 2004). Atlantic Water from the Arctic Ocean is largely excluded by the shallow sills in these channels. The Atlantic Water that reaches northern Baffin Bay is carried in the West Greenland Current; it submerges beneath the Polar Water when reaching the northern Baffin Bay (Tang et al., 2004). Sea ice covers nearly all of Baffin Bay in winter; it begins to form in September and reaches maximum coverage in March. It is thickest along Baffin Island, where the flow of the low salinity Arctic surface water is concentrated. However, the ice arches that form in Nares Strait in most years block passage of sea-ice floes from the Arctic Ocean and facilitate the formation of the North Water Polynya, a large area of thin to absent sea ice that encompasses the core sites in Smith and Lancaster sounds (Dunbar, 1969; Melling et al., 2001; Tang et al., 2004).

NE GREENLAND SHELF

The investigated sites off NE Greenland are today characterized by chilled Atlantic Water returning southward along Greenland as a subsurface water mass that originated in the North Atlantic Drift and either returns southward off Svalbard or as a subsurface flow of Atlantic Water that has circuited the Arctic Ocean (Aagaard & Coachman, 1968a, b). The relatively warmer Atlantic-source waters reached to the glacier tongues of NE Greenland through deep channels (Schaffer et al., 2019). Atlantic Water is overlain by Polar surface water from the Arctic Ocean (East Greenland Current; Aagaard & Coachman, 1968a, b) combined with locally formed surface water from melting of the Greenland ice sheet. One of our sites is located close to Zachariae Isbrae, while the second site is located farther offshore. Zachariae Isbrae likely extended much further onto the shelf and closer to the study sites during the deglaciation and the early Holocene (Larsen et al., 2018).

MATERIALS AND METHODS

During the Petermann Glacier Expedition of Swedish Icebreaker Oden in 2015, the uppermost 1 to 2 cm of seafloor sediments were collected for foraminiferal analysis from 12 multicores at 11 sites as well as from the top 2 cm of two modified Uwitec cores raised from beneath the floating ice tongue (cf., Makinson & Anker, 2014). The present water depths ranged from 517 to 1041 m (Fig. 1B), the bottom water temperatures between 0.27 to 0.3°C, and bottom salinities from 34.77 to 34.82 psu. Sample volumes ranged between 6 and 35 ml. Immediately after sampling the multicore tops on deck, a buffered solution comprising 70% distilled water and 30% alcohol, by weight, 1 g baking soda and 1 g of Rose Bengal (dichlorotetraiodofluorescein) stain was added to the vials to preserve the foraminifera and to stain living specimens. The samples were immediately refrigerated. In addition to the surface samples, numerous sediment cores, representing the upper 10 m of the sediment section, were split and described during the cruise. As part of the core-description process, very small samples were routinely sieved at 0.063 mm to observe the faunal content with depth in the cores. The new species, Glomulina oculus, was commonly observed during this process.

Foraminiferal analysis of the surface samples was completed in the Micropaleontology Laboratory at INSTAAR, University of Colorado. The stained samples were washed through a 0.063-mm mesh sieve. The >0.063 mm fraction was stored in a buffered solution (70% distilled water and 30% alcohol, by weight, and 1 g baking soda) to keep the pH >8 and <<9. Analysis of these foraminiferal samples was carried out in the buffered solution in a foraminiferal picking tray under a binocular microscope. Both living (Rose Bengal stained) and dead (unstained) specimens were counted and are reported as total assemblages herein. In order to determine whether *G. oculus* would be preserved using a dry

sample analysis, we also wet-sieved sediment from equivalent samples that had been freeze-dried, and subsequently we oven-dried the >0.063-mm fraction at 25°C. *Glomulina oculus* was found both in wet and freeze-dried samples.

Photographs of specimens in the storage solution were taken, and specimens were picked from wet and dry samples using a brush, allowed to dry, stored on cardboard slides and photographed. Specimens picked from the buffered solution were rinsed in distilled water before placing them on slides. The specimens were sent to Aarhus University for scanning electron microscope (SEM) photomicrographs. Here the gold-coated specimens were photographed using a Versa 3D FIB-SEM at the iNANO Cryo-Electron Microscopy Facility.

Fossil samples from sediment gravity core Hly03-05GC from Hall Basin (81.621°N, 63.26°W; 797 m water depth) were prepared by freeze-drying, followed by sieving and then air drying of the 0.063 mm sediment (Jennings et al., 2011). For piston core 2001LSSL-014PC in northern Baffin Bay (77.702°N, 75.07°W; 658 m water depth), the wet procedure used for the modern OD1507 samples was used to study the foraminifera (Jennings et al., 2019). The age control for these two cores was based on radiocarbon dating of benthic and planktonic foraminifera, and the resulting age control and the procedures used to generate age models and calibrate the ages all are presented in respective publications. The sand percentages from surface samples in northern Nares Strait and northern Baffin Bay were obtained using the Malvern Mastersizer 3000 laser diffraction particle size analyzer (cf., Jennings & Andrews, 2019; Jennings et al., 2019) whereas weight% sand data from the Hly03-05GC (Hall Basin) was obtained by weighing the sieve fractions used for foraminiferal analysis (Jennings et al., 2011).

Foraminiferal and grain-size samples from the cores in northern Baffin Bay (2008029-49PC: 74.026°N, -77.13° W; 868 m water depth; 2008029-59PC: 74.258°N, 82.23°W, 791 m water depth; 2001LSSL-14PC were treated with the same methods as those for the OD1507 samples.

Samples from gravity core DA17-NG-ST07-73G (79°04.100′N, 11°54.191′W; 385 m water depth) and Rumohr core DA17-NG-ST08-90R (78°30.001′N, 17°18.431′W; 594.9 m water depth) from the Northeast Greenland shelf were prepared at the Department of Geoscience, Aarhus University, through wet-sieving of the sample on 0.063-mm and 0.1-mm sieves. After sieving, the samples were dried prior to analyses.

ECOLOGY AND PALEOENVIRONMENTS

MODERN SAMPLES IN NORTHERN NARES STRAIT AND OFF NE GREENLAND

Glomulina oculus n. sp. was found in every surface sample collected in northern Nares Strait and the Petermann Fjord, including in surface sediment samples from beneath the ice tongue, where 1 and 2 dead specimens were found in 006 and 001 UW, respectively (Fig. 1B). It was found at abundances ranging from close to zero to nearly 50 specimens per ml of sediment with ratios of living to total counts ranging between 0 and 0.9 (Fig. 3). Sediment accumulation rates in Petermann Fjord were estimated at 0.3–1 cm from ²¹⁰Pb

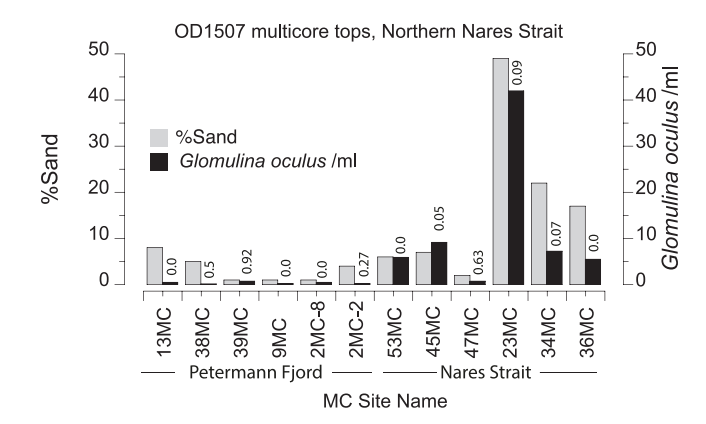


FIGURE 3. Glomulina oculus specimens per ml of sediment sample compared to the weight percentage of sand at each multicore site. Numbers above the G. oculus/ml bars represent the ratio of living (Rose Bengal stained) counts to total counts of G. oculus (note that a value of 1 indicates that all of the specimens were living, while a value of 0 indicates that all specimens were dead at the time of collection. Sand percentage data are not available for the Uwitec core tops so the two sub-ice tongue sites are not included in the figure.

analysis with an overall Holocene rate from radiocarbon-based analyses of 0.06 cm a⁻¹ (Reilly et al., 2019). There is a tendency for the samples with higher percentages of sand (>0.063 to <1000 mm) to have higher numbers of specimens of *G. oculus* (Fig. 3). Samples outside of the Petermann Fjord, except for 47MC, tended to have greater sand percentages and greater abundances of *G. oculus* (Fig. 3).

Glomulina oculus was present at under 2% of the total (calcareous and agglutinated) benthic foraminiferal assemblages, except at two sites in Hall Basin near the mouth of the Petermann Fjord. At these two stations (multicores 47MC and 23MC), G. oculus occurred at 6.4 and 15.4% of the total benthic foraminiferal assemblage, respectively (Fig. 4). Figure 4 shows the additional species that occur at >5% of the assemblage at these two sites. *Elphidium clavatum* (Cushman) (cf., Darling et al., 2016) is the most abundant species, making up 37.7% and 26.5%. Cassidulina neoteretis Seidenkrantz, Nonionella iridea Heron-Allen and Earland, Stetsonia horvathi Green and the agglutinated species Textularia earlandi Parker are also common at both sites. Epistominella arctica Green makes up 12.3% of the assemblage in 23MC but is absent in 47MC. The high percentages of E. clavatum are consistent with the outflow of glacial meltwater (Hald & Korsun, 1997, as E. excavatum) from the Petermann Glacier that is documented to be most prominent along the Greenland side of Hall Basin (Heuzé et al., 2017; Washam et al., 2019). Taken together, the other calcareous species are consistent with the modern environment of a stratified water column with chilled and modified Atlantic Water underlying Polar Water in an environment with seasonally mobile sea-ice cover that allows episodic marine productivity (e.g., Wollenburg & Mackensen, 1998; Jennings et al., 2004).

Glomulina oculus is also present, albeit not abundant, in muddy surface sediments from a Rumohr core DA17-NG-ST08-90R (594.9 m water depth; Fig. 1A; data not shown) taken from the deeper, inner part of a trench extending from the glacier tongue of Zachariae Isbrae to the shelf edge of NE Greenland. The dominant species of the assemblage is

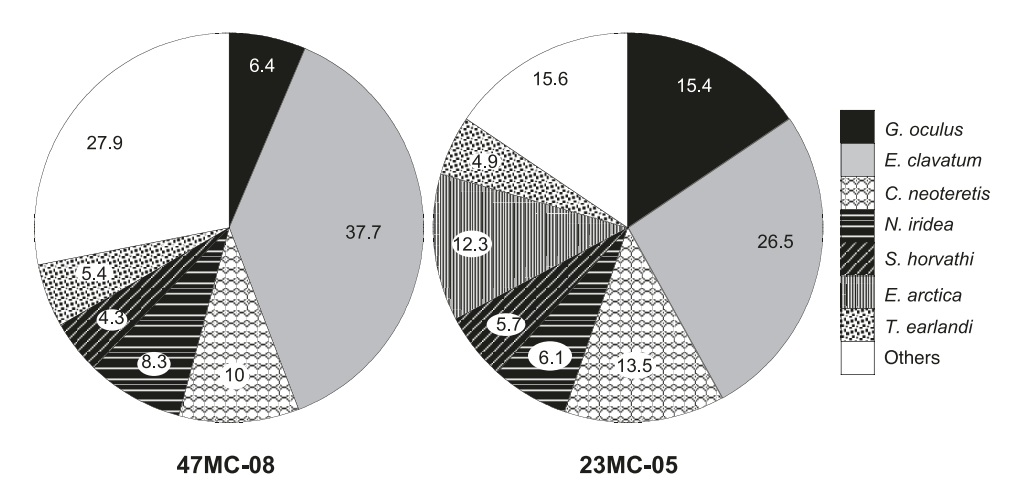


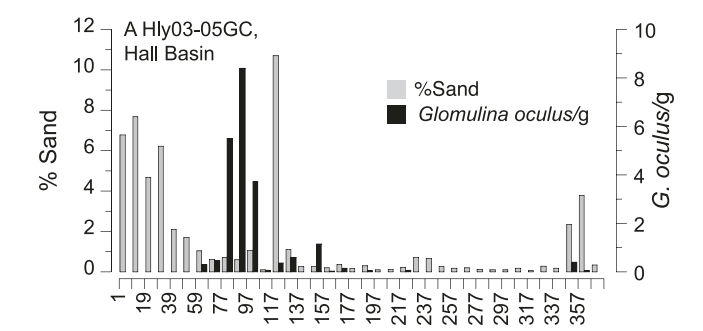
FIGURE 4. Glomulina oculus and other benthic foraminiferal species that occur at >5% in multicore surface samples at 47MC and 23MC outside of the Petermann Fjord (see Fig. 1B for locations).

Cassidulina neoteretis (data not shown). Chilled return Atlantic Water is flowing along the sea floor through this deep trench, while surface waters are characterized by Polar Water from the East Greenland Current (Aagaard & Coachman, 1968a, b; Schaffer et al., 2019). The site is normally covered by perennial sea ice, but unusually low sea-ice cover in late September 2017 allowed us to reach this site; the core was taken from right at the sea ice edge off the glacier.

Occurrences of GLOMULINA occulus in Holocene Sediment Cores

Glomulina oculus n. sp. has been found in several sediment cores, among those are two cores with published foraminiferal faunal data (Jennings et al., 2011, 2019). However, specimens of *G. oculus* have hitherto been assigned to other taxa. In both previously published cores, the absolute abundances, as well as relative frequency of *G. oculus*, are at a maximum in or close to intervals with relatively high sand contents that are associated with transitional environments related to deglaciation (Figs. 5, 6).

In core Hly03-05GC from Hall Basin (Fig. 1A, B), the region that supports the occurrence of G. oculus today, it was misidentified as Miliolinella subrotunda (Montagu) by Jennings et al. (2011) because of its similar appearance to juveniles of this species. In Hly03-05GC, G. oculus was present in very low percentages in several samples of the distal glaciomarine laminated clay that was deposited in front of the confluent Greenland and Innuitian ice sheets (Jennings et al., 2011). However, its percentages increased greatly in the sediments encompassing the transition from a glacial embayment to the open strait that followed ice retreat, but the species did not occur in sediments above this interval (Fig. 6A). In the early Holocene interval between \sim 7 and 10 cal ka BP, where G. oculus is found, it is associated with C. neoteretis as the most dominant species, suggesting presence of chilled Atlantic Water (e.g., Seidenkrantz, 1995; Jennings & Helgadottir, 1994). Oridorsalis umbonatus (Reuss) increases near the top of the laminated mud unit and continues into the base of the bioturbated mud unit. Its occurrence was interpreted to reflect deeper connection to the Arctic Ocean due to isostatic depression immediately after glacier recession (Jennings et al., 2011), and it also likely reflects low food supply during initial deglaciation (Osterman et al., 1999). Increasing percentages of *E. clavatum* and *N. iridea* suggest more open water that promoted greater marine productivity during deposition of the bioturbated mud that closely followed opening of the strait (Gooday & Hughes, 2002; Fig. 6A).



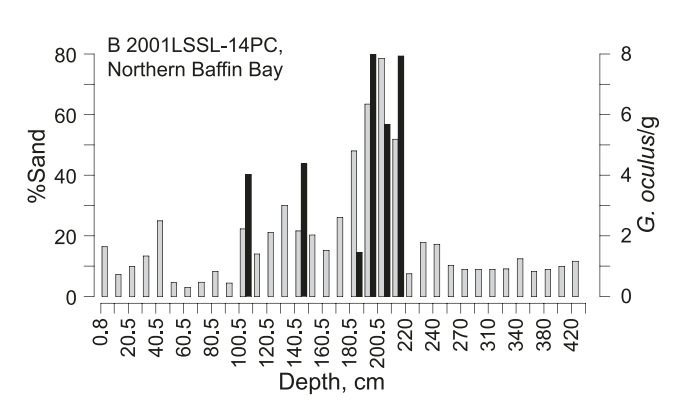


FIGURE 5. Glomulina oculus specimens per g of sediment sample compared to the weight percentage of sand downcore in A Hly03O5GC from Hall Basin, and **B** in 2001LSSL-14PC from northernmost Baffin Bay. Data from Jennings et al. (2011, 2019).

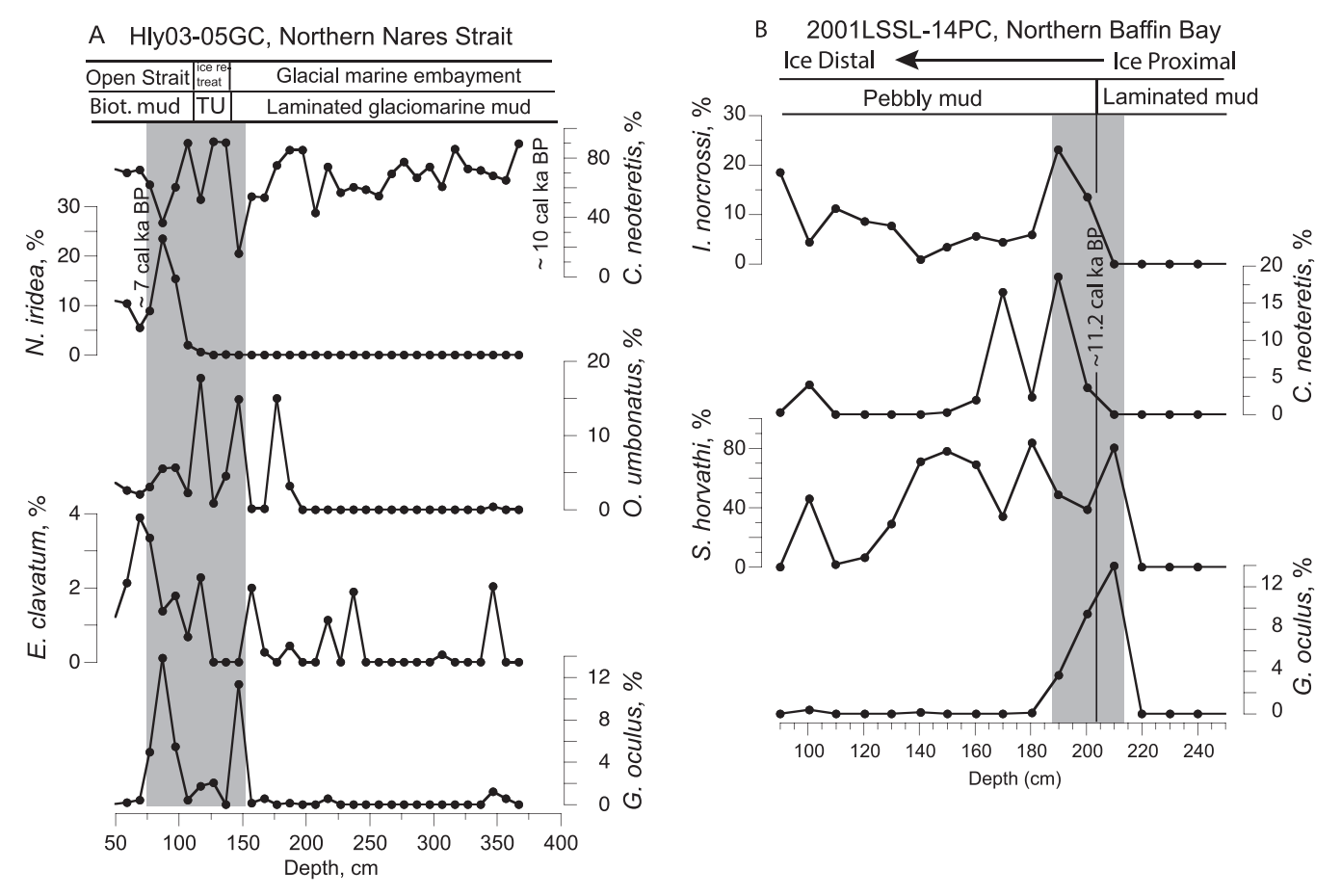


FIGURE 6. Downcore percentages of *Glomulina oculus* and other important species in key intervals of **A** Hly03O5GC from Hall Basin, and **B** in 2001LSSL-14PC from northernmost Baffin Bay. Data from Jennings et al. (2011, 2019).

Glomulina oculus also was found in sediment core 2001LSSL-014PC in northern Baffin Bay, just south of Smith Sound (Fig. 1A; incorrectly named as *Cyclogyra* sp.), in the very first fossiliferous samples of glaciomarine sediments above a till. Its occurrence was limited to the top of a sediment facies of laminated ice proximal glaciomarine sediments (L2, Jennings et al., 2019) and the base of overlying pebbly mud (L3, Jennings et al., 2019) deposited at \sim 11.2 cal ka BP during calving margin ice retreat, prior to the opening of Nares Strait (Fig. 6B). The sedimentation rate in this interval is estimated at 0.13 cm a^{-1} . Across this interval in the core, G. oculus is associated with high percentages of S. horvathi, a species common in the Arctic Ocean that is indicative of low food supply and heavy seaice cover. As in Hly03-05GC, it is associated with the chilled Atlantic Water species C. neoteretis, but it also co-occurs with the (sub)Arctic species *Islandiella norcrossi* (Cushman), a species that is indicative of stable bottom salinities and highly chilled Atlantic Water (Lloyd, 2006; Fig. 6B).

True to its association with transitional glacial marine environments, abundant *G. oculus* has also been found in glaciomarine sediments closely overlying a till in two cores from Lancaster Sound (data not shown): 2008029-49PC (868 m water depth) and -59PC (791 m water depth) (Paratype from 59PC illustrated in Figure 7.7). A few spec-

imens have also been identified in early Holocene (ca 8–9 cal ka BP) sediments of core DA17-NG-ST07-073G on the NE Greenland shelf (385 m water depth; data not shown). These sediments were deposited just above sediments rich in reworked foraminifera from the Pliocene or early Pleistocene, indicating a period of sediments being flushed out during the deglacial retreat of the Greenland ice sheet.

Given the fact that we have now identified the species in several surface sediment samples and cores from two geographically separate regions, we suspected that G. oculus has not been previously reported because it might have low preservation potential or be too fragile to survive the common practice of drying foraminiferal samples prior to sieving. Consequently, we tested its preservation potential in two ways. First, we sieved previously freeze-dried samples from multicore tops 23MC and 45MC that were known to have relatively high numbers of the species when prepared with the wet procedures. We found that G. oculus in these paired samples not only survived freeze-drying, they also were present after oven drying at 25°C. In fact, several examples of these dried specimens were picked for SEM imaging. In core Hly03-05GC, the foraminiferal samples were prepared by freeze-drying followed by sieving at 0.063 mm and then air-drying of the 0.063 mm sediment fraction. The presence of G. oculus in these samples shows that the species is preserved after drying, and its presence/absence does not rely on the wet technique. It seems likely that *G. oculus* has been observed at more sites than we are currently aware of, but that it has been left unidentified or has been assigned to other genera and species as was the case for the studies of cores Hly03-05GC (Jennings et al., 2011) and 2001LSSL-014PC (Jennings et al., 2019). *Glomulina oculus* has not to our knowledge been described or illustrated previously.

In summary, based on its modern occurrences in northern Nares Strait, Glomulina oculus is a (high) Arctic benthic foraminiferal species that lives in areas of perennial to mobile sea ice beneath a stratified water column with chilled Atlantic Water, overlain by Atlantic Water mixed with glacier meltwater, all overlain by Polar Water from the Arctic Ocean. Elevated abundances of G. oculus are associated with increased sand content, probably originating from sea ice and iceberg rafting into relatively high currents or possibly by sand delivered through other disturbance processes. Its peak occurrences in transitional glaciomarine facies farther south in northernmost Baffin Bay, Lancaster Sound and NE Greenland shelf, but absence from modern samples in these areas, suggest that the glaciomarine association is pre-eminent, but the specific conditions that produce G. oculus peaks are not yet well understood.

SYSTEMATIC DESCRIPTION

Suborder MILIOLINA Delage & Hérouard, 1896 Family FISCHERINIDAE Millett, 1898 Subfamily GLOMULININAE Saidova, 1981 Genus *Glomulina* Rhumbler, 1936

Glomulina oculus n. sp. Figs. 7–11

The subfamily Glomulininae is characterized by a test with proloculus followed by a streptospirally enrolled tubular chamber; later chambers are one-half coil in length. The genus *Glomulina* has a globular test and a proloculus followed by a streptospirally enrolled, undivided tubular second chamber. Later chambers are one-half coil in length. Aperture rounded, at the end of the last chamber.

Deriviato Nominis/Deriviation of name. From oculus (Latin) = eye. Refers to the round or eye-like design of specimens when seen in side view.

Diagnosis. Small oblong, globular to discoidal miliolid, normally with a large proloculus followed by 2–4 tubular chambers, most commonly 2–3, each of about ½ to ¾ of a whorl. The aperture at the open end of the last tubular chamber is open and semicircular.

Holotype. Three-chambered specimen from OD1507-23MC-5, 0-2 cm. U.S. National Museum Paleobiology catalog number USNM PAL 726877 is housed at the Smithsonian Institution, Washington, D.C., U.S.A. (Figs. 7.2a, b).

Paratypes. Thirteen specimens housed at the Smithsonian Institution, Washington, D.C., U.S.A. Paratypes 1, 2 (3 chambers; USNM PAL 726878 and 726879) and Paratype 3 (4 chambers; USNM PAL 726880) from OD1507-23MC, 0–2 cm. Paratypes 4–7 (3 chambers; USNM PAL 726881, 726882, 726883, and 726884) and Paratype 8 (4 chambers; USNM PAL 726885) from OD1507-45MC-5, 0–1 cm. Paratypes 9–11 (3 chambers; USNM PAL 726886, 726887,

and 726888) from 2008029-59PC, 549-551 cm (Fig. 7.7). Paratypes 12 and 13 (5 chambers; USNM PAL 726889 and 726890) from OD1507-34MC-1, 0–2 cm (Fig. 7.6).

Material. Early Holocene to Recent; northern Nares Strait, northern Baffin Bay, NE Greenland shelf.

Type locality. Hall Basin, northern Nares Strait.

Type level. Recent; early Holocene.

Description. Test discoidal to globular, round to slightly elongate with 3-4 chambers primarily organized in one plane, but with tendency for the third and fourth chambers to be formed slightly off-center from the periphery (i.e., weakly streptospiral). The species has a large, spherical proloculus followed by normally two or three tubular chambers. The proloculus is wrapped by the first tubular chamber of $\sim \frac{1}{4}$ of a whorl in length. The third chamber makes up \sim ³/₄ of a whorl with a slight change in the coiling plane (i.e., slightly streptospiral) as it completes the encircling of the proloculus (Figs. 7.1a, b, c). Most specimens are found with only three chambers (Figs. 7.1, 7.2, 7.3, 7.5, 7.7). If a fourth chamber is present, it encircles the test for ½ of a whorl in nearly the same plane as the first whorl, but, as for the third chamber, with a tendency to deviate from planispiral (Fig. 7.4). Rare specimens with five chambers have been found (Fig. 7.6). The fifth chamber is added far from the original nearly planispiral plane, making the fivechambered specimens look nearly quinqueloculine. A few two-chambered individuals have also been observed. Each tubular chamber embraces the preceding chambers in an evolute chamber arrangement, causing the proloculus to be visible always, although more of the proloculus is hidden with the addition of more chambers. In specimens with three chambers, a larger section of the proloculus is visible (Fig. 7.1) than in specimens with four (Fig. 7.4) and five chambers (Fig. 7.6). The cross-sectional shape of the tubular chambers is partly compressed with the cross section of the tube tending towards semicircular. Sutures are relatively distinct and accentuated by the fact that often the diameter of the tubular chamber decreases lengthwise, but increases distinctly from one chamber to the next, making the tube diameter different at each side of the suture.

The aperture at the open end of the last tube is rounded, semicircular in shape and fully to near-fully open (Figs. 7, 8, 9, 10). Scanning electron microscope images reveal a low thickened bulge or 'bump' in the middle of the apertural base, stretching a little from the aperture opening inwards into the last chamber, making the bulge longer than wide and it gradually becomes lower inwards into the test, thus forming a more steep outer end and a less steep inner end of the bulge (Fig. 10). This slight bump at the base of the aperture is also sometimes visible in light microscopy (Figs. 7.2b, 7.5).

Wall structure is calcareous, imperforate, porcelaneous, but commonly semi-translucent. In scanning electron microscope (SEM) analyses, a clearly porcellaneous wall structure (Fig. 11) may be observed with the outer layer (the extrados, see Parker, 2017) of aligned calcareous crystal needles primarily ordered lengthwise in direction of the chambers (Figs. 11.1, 11.2). Below the extrados, the main body of the wall (porcelain; see Parker, 2017) consists of randomly orientated crystal rods, shorter and thicker than those of the extrados and intrados (Figs. 11.3a, b). Also noteworthy is

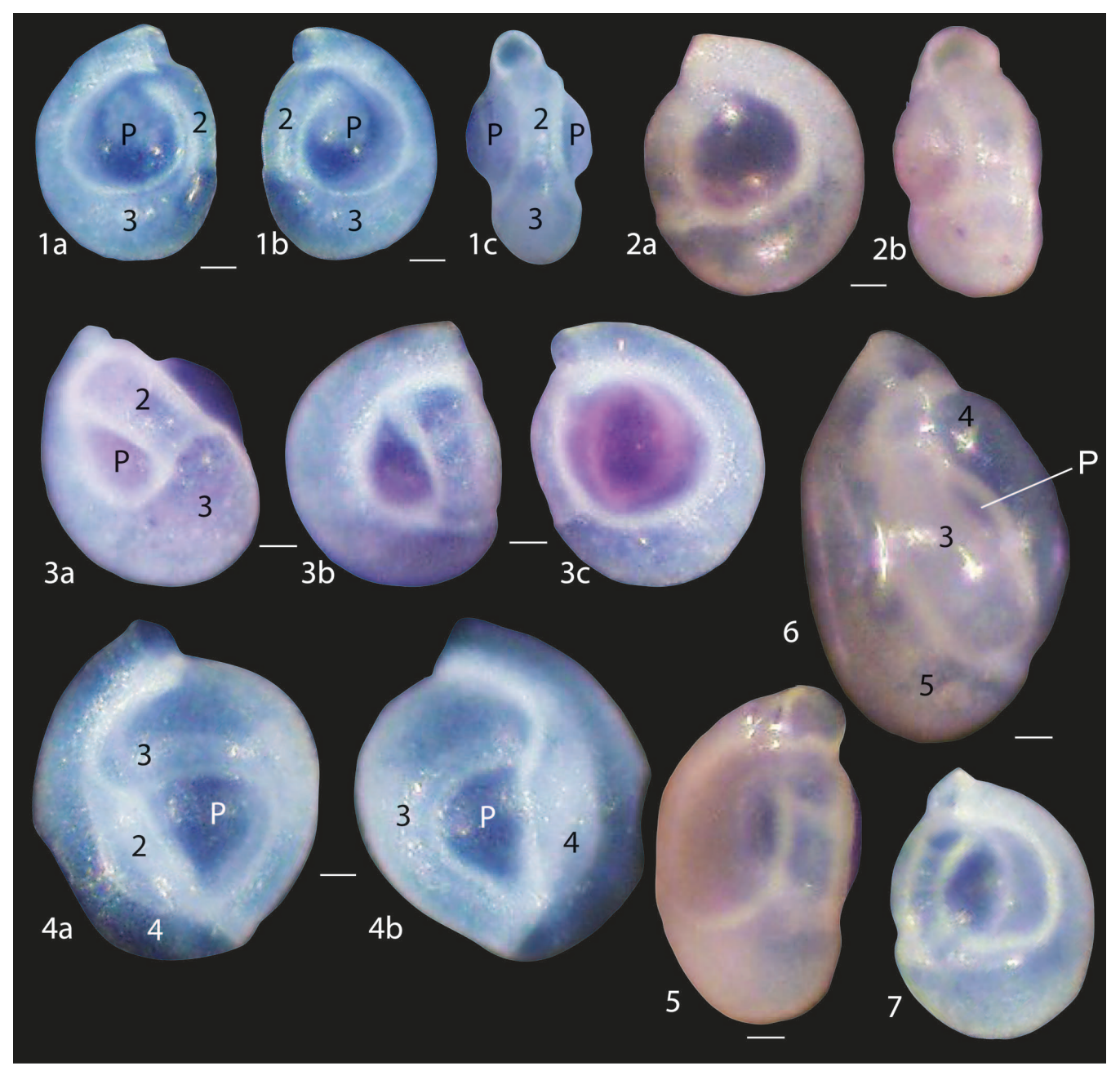


FIGURE 7. Examples of *Glomulina oculus* from OD1507 multicore (MC) surface sediments (1-6) and a fossil specimen (7) as light microscope photographs. **1a, b** side views, **1c** apertural view of three-chambered specimen from 47MC showing nearly planispiral chamber arrangement with chambers numbered from proloculus (P), i.e., first chamber, and onwards. **2a** Side view and **2b** apertural view of Holotype (USNM PAL 726877) from 23MC. **3a, b, c** Side views of stained three-chambered specimen (live) showing pronounced streptospiral third chamber that obscures the proloculus on one side. **4a, b** Side views of four-chambered specimen from 47MC; chamber 2 is obscured in 4b. **5** Apertural view of three-chambered specimen from MC47 showing the small 'bump' at the base of the aperture. **6** Paratype (USNM PAL 726889), five-chambered specimen from 34MC; chamber 2 is not visible. **7** Paratype USNM PAL 726886), fossil specimen of typical three-chambered form from 2008029-59PC, 549-551 cm, All specimens at the same scale. Scale bars = $20 \mu m$.

that in a single specimen, we were able to observe the crystal structure of the inner layer (intrados; see Parker, 2017) within the proloculus (Figs. 11.6a, b, c). Here the crystal needles were also randomly oriented, but the crystals were covered by a fine surface layer with fine wavy ridges. This very thin layer inside the proloculus is presumably part of a thin organic layer covering the calcareous crystal needles of the

intrados. The ridges have a swirling pattern, reflecting the round shape of the proloculus (Figs. 11.6a, b).

Despite the fact that the specimens, which were scanned, were collected from the upper 2 cm sediment, they already showed some dissolution of the shell, and in some specimens the early chambers also showed re-crystallization of the carbonate forming rhomboid crystals at the surface of

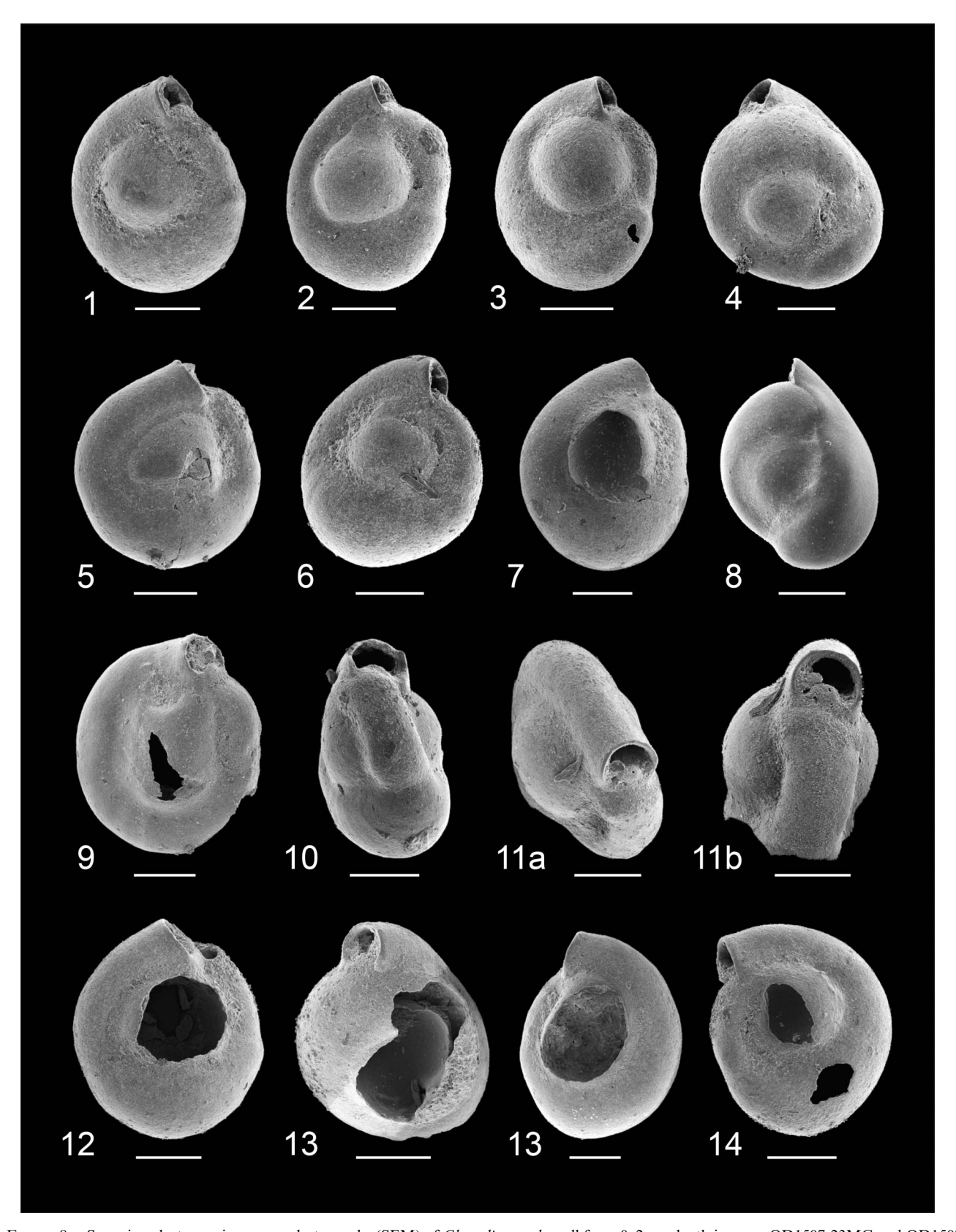


FIGURE 8. Scanning electron microscope photographs (SEM) of *Glomolina oculus*, all from 0–2 cm depth in cores OD1507-23MC and OD1507-47MC. 1 Specimen SEM16. 2. Specimen SEM2. 3 Specimen SEM3. 4 Specimen SEM1. 5 Specimen SEM17. 6 Specimen SEM5. 7 Specimen SEM15. 8 Specimen SEM6. 9 Specimen SEM10. 10 Specimen SEM11. 11a, Marginal view of specimen SEM14, note the very large proluculus that is clearly visible on both sides on the 11b view. 12 Specimen SEM12 with proloculus broken on both sides. 13 Specimen SEM4 with a clear view of the inner wall of the proloculus. 13 Specimen SEM13 with proloculus broken on upper side. 14 Specimen SEM8. Scale bar = $50 \mu m$.

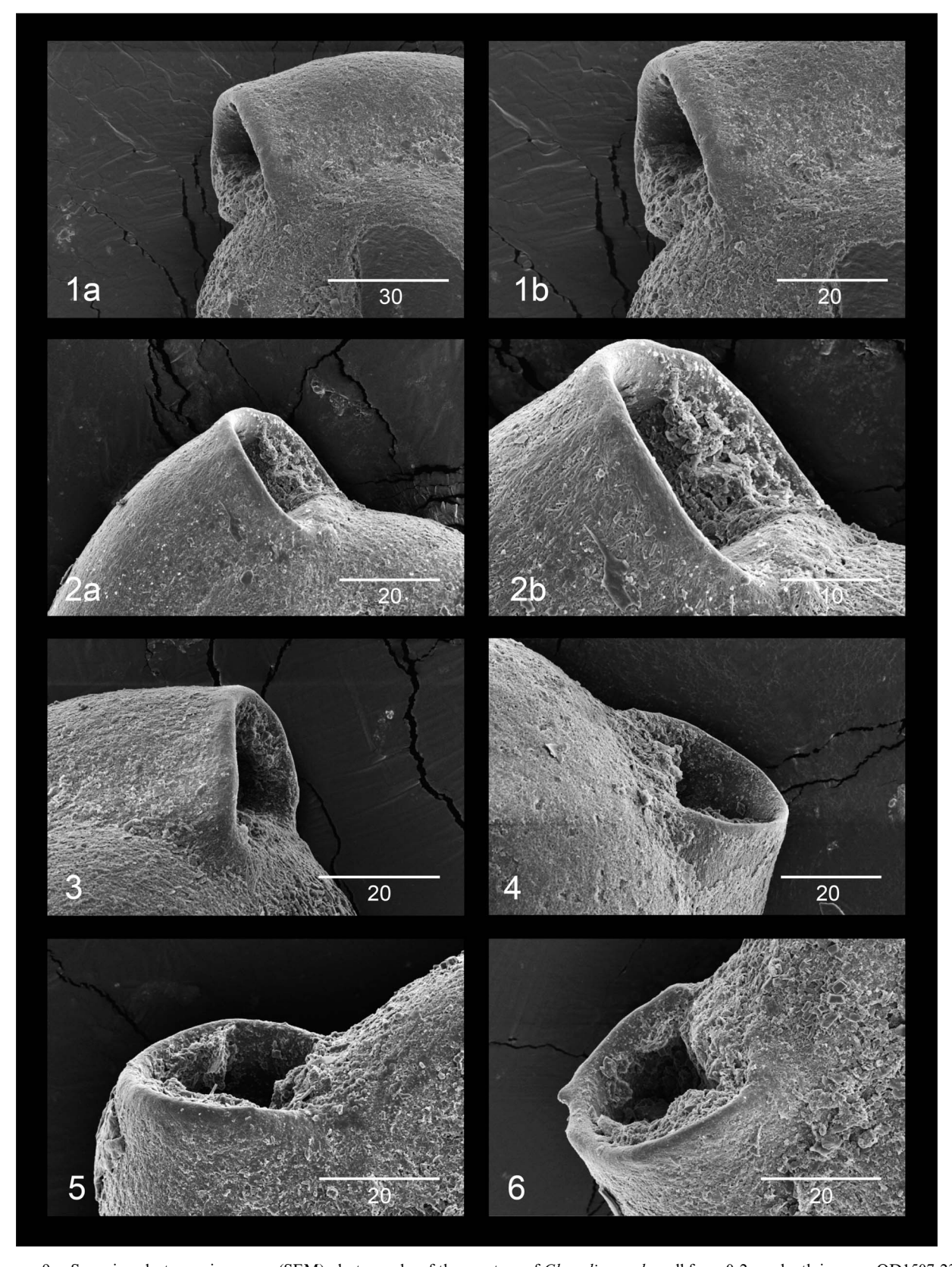


FIGURE 9. Scanning electron microscope (SEM) photographs of the aperture of *Glomolina oculus*, all from 0-2 cm depth in cores OD1507-23MC and OD1507-47MC. 1a Overview of aperture of specimen SEM8. 1b Detailed view of aperture of Specimen SEM8. 2a, b Specimen SEM2. 3 Specimen SEM3. 4 Specimen SEM1. 5 Specimen SEM5. 6 Specimen SEM16. Scale bar = 10–30 μm.

229

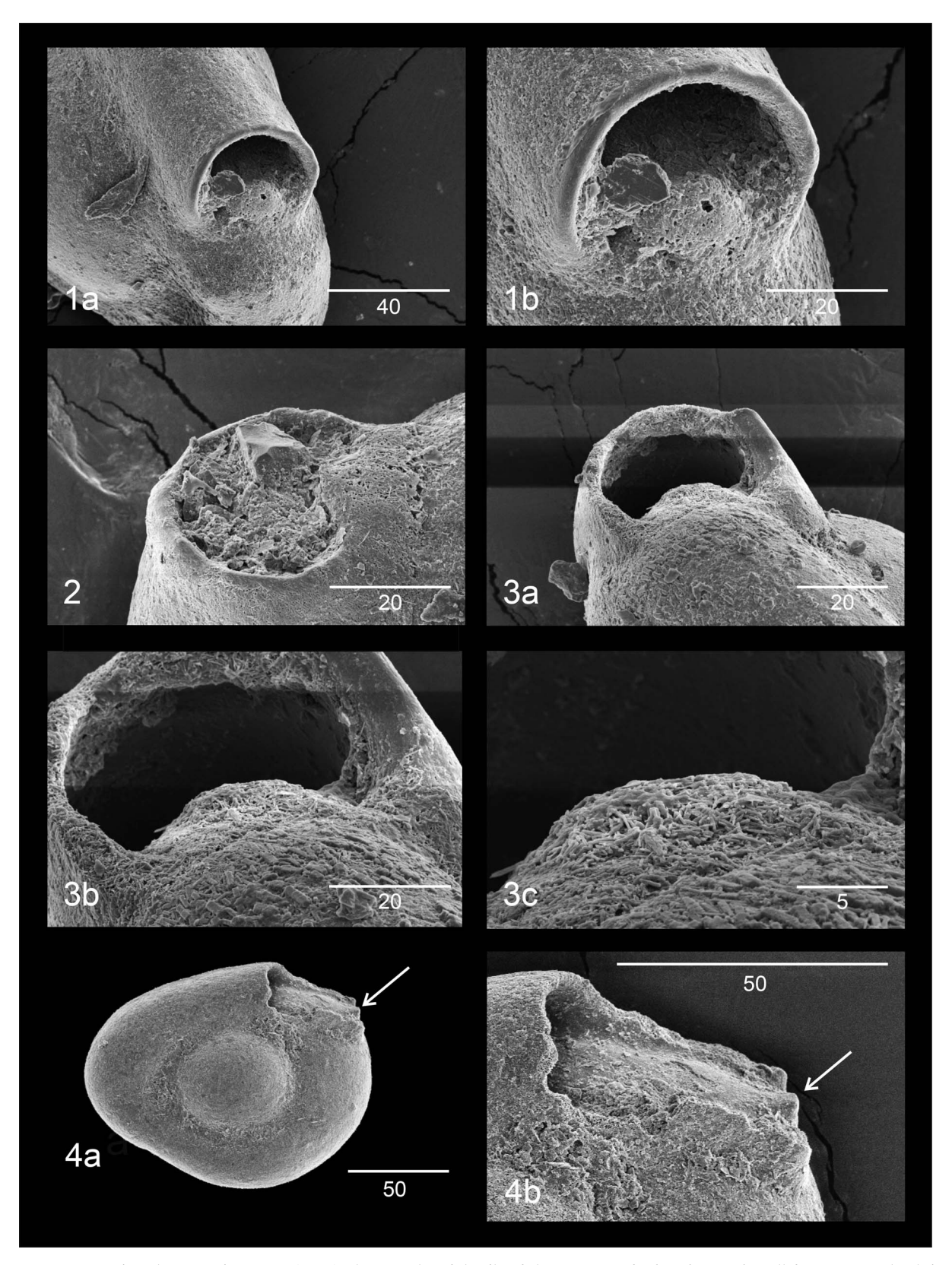


FIGURE 10. Scanning electron microscope (SEM) photographs of details of the aperture of *Glomolina oculus*, all from 0-2 cm depth in cores OD1507-23MC and OD1507-47MC. **1a, b** Overview and detailed view, respectively, of aperture of Specimen SEM14. Note the clear bulge at the base of the aperture. **2** Aperture of specimen SEM10, with aperture filled with sediment and carbonate crystals. **3a, b** Apertural view of specimen SEM11. **3c** Detailed view of the bump at the base of the aperture of specimen SEM11. Note the wall structure of randomly oriented calcite needles. **4a, b** Overview and detail of aperture, respectively, of specimen SEM7. The last part of the last chamber is broken off providing a side view of the bump at the base of the apertural opening (marked with arrow); the abrupt outer side and tapering internal side of the bump are clearly seen. Scale bar = 5–50 μm.

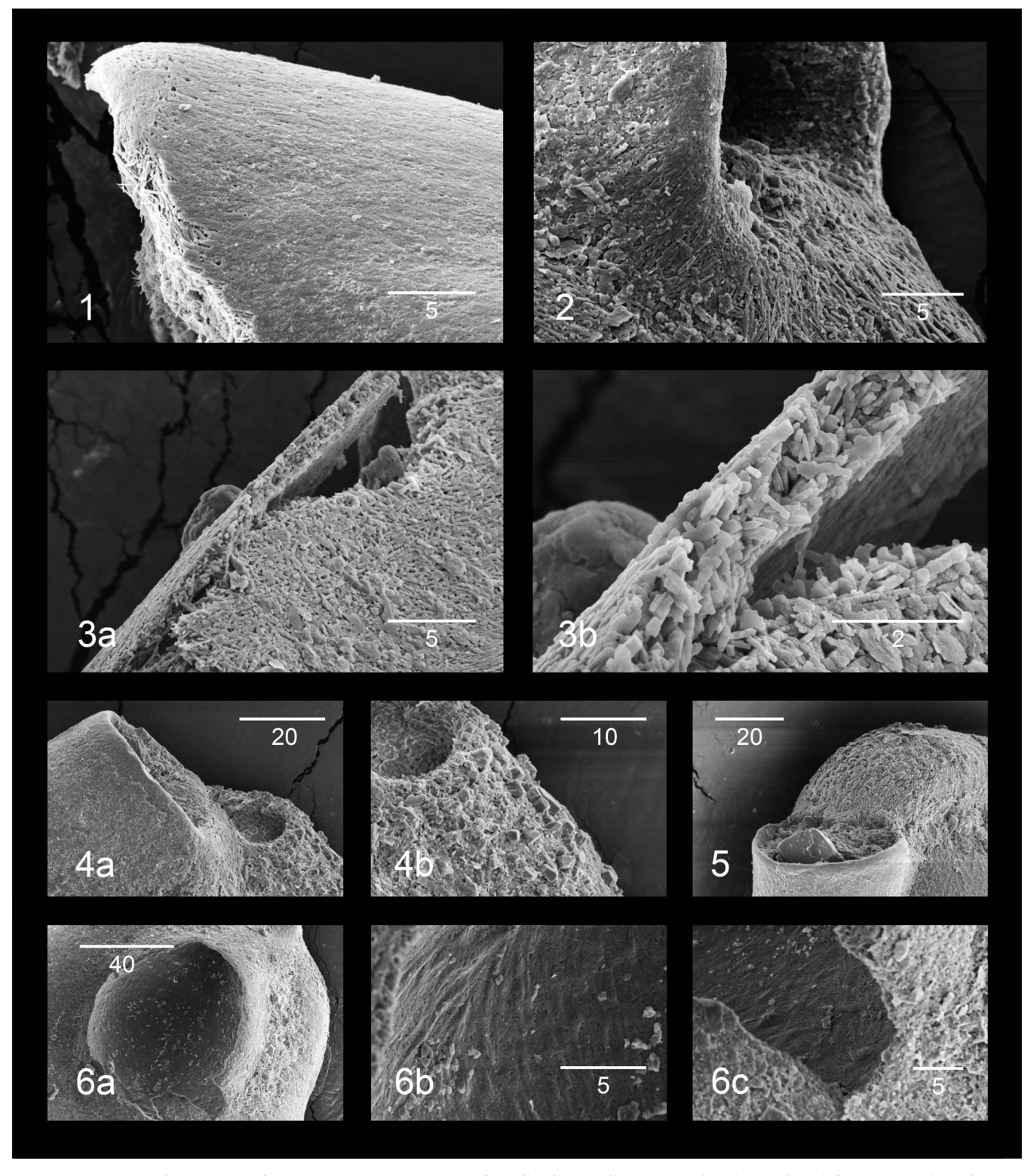


FIGURE 11. Scanning electron microscope (SEM) photographs of details of test wall structure *Glomolina oculus*, all from 0–2 cm depth in cores OD1507-23MC and OD1507-47MC. 1 Broken end of the last chamber of specimen SEM6 showing the thin layer of oriented crystals of the extrados, and at the end the randomly oriented needles the middle section of the test wall (porcelain). 2 The crystals are lengthwise orientated near the aperture. 3a, b Broken test wall showing the randomly oriented crystals of the porcelain (central) part of the wall. 4a, b, 5 Larger calcite crystals seen at the base of the aperture, presumably indicating post-mortem re-crystallization of this older part of the test in specimens SEM12 and SEM17. Note that the upper end of the second chamber of specimen SEM 12 is broken providing a view inside the second chamber. The large crystal seen in the apertural opening of SEM17 is considered a post-mortem feature not relevant for the species description. 6a, b, c Detailed view of the inner wall of the proloculus of specimen SEM 15. 6a, b shows the randomly orientated crystals of the middle (porcelain) section of the wall covered by a thin inner (intrados) wall section with ridges in an irregular, swirly pattern. Scale bar = 5–40 μm.

GLOMULINA OCULUS N. SP. 231

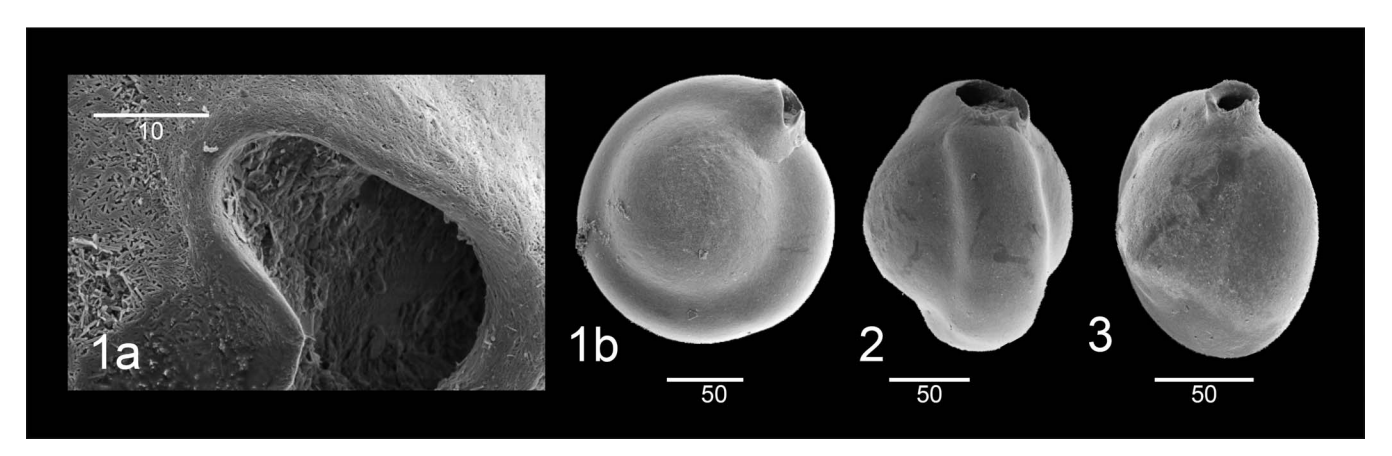


FIGURE 12. Scanning electron microscope (SEM) photographs of *Cornuspira distincta* and a juvenile specimen of *Miliolinella subrotunda*, all three specimens from 440–441 cm core depth (Marine Isotope Stage 3 in age) in gravity core DA12-11/2-GC03 (60°78238'N, 9°79373'W; 742.4 m water depth) south of the Faeroe Islands. 1a Detail of aperture of *C. distincta* specimen SEM2-2. 1b *C. distincta* specimen SEM2-2. 2 *C. distincta* specimen SEM2-3.

the test (Figs. 11.4, 11.5). None of the specimens analyzed in the SEM were stained, indicating that they were all dead at the time of collection.

Dimensions. Average test dimensions with details listed in Table 1: 161 by 131 μ m for three-chambered tests, 196 by 168 μ m for four-chambered tests, and 242 by 154 μ m for five-chambered tests (Table 1).

Variation. There is relatively little variation within this species, but the number of chambers varies from two to five, including the proloculus (Fig. 7). Three-chambered specimens are the most common. In specimens with four chambers, less of the proloculus is exposed on one side, while in five-chambered specimens, the proloculus is mostly obscured. Smaller specimens tend to have a semicircular shape in side view, while the largest specimens are more elliptical in shape (side view).

Affinities. Glomulina oculus is distinguished from Glomulina fistulescens Rhumbler (1936), type species of Glomulina from the Kiel Bight, Germany, by its generally significantly fewer chambers (none of the specimens depicted in the type description of Glomulina fistulescens have less than five chambers, while 5-chambered G. oculus are rare), resulting in a flatter shape of the G. oculus test. Glomulina oculus differs from Glomulina rotiensis Loeblich & Tappan (1994) from the western Timor Sea by its rounder aperture and its more distinct suture between the proloculus and the 2–3 surrounding chambers, giving G. oculus a more uneven, flattened quatrefoil shape in peripheral view (Figs. 7.1c, 8.10, 8.11b), than the more smoothly rounded Glomulina rotiensis.

Glomulina oculus has a superficial resemblance to Cornuspira distincta (Cole & Scott) (originally described as Cyclogyra distincta in Scott et al., 2008) that has a similar shape with a large round proloculus followed by a long planispiral to slightly streptospiral tube (Fig. 12.1-2). However, G. oculus is clearly distinguished from C. distincta by having at least three chambers, while C. distincta has only two chambers, and the specimens of C. distincta are generally much more well-rounded in side view than G. oculus (Fig. 12.3). In addition, the aperture of *C. distincta* is rather triangular with a basal plate in contrast to the semicircular aperture without any distinct basal plate in G. oculus. The apertural shape and basal plate of C. distincta is clearly seen in the figures of the original description of C. distincta, and we were able to confirm this when investigating specimens under light microscope and in SEM microphotographs (Fig. 12.1). Among the specimens that we studied are those originally described as Cyclogyrinae by Bergsten (1994) from surface sediment samples from the Yermak Plateau (i.e., the same material that contained the specimens assigned as lectotypes for C. distincta by Scott et al., 2008). We have not been able to test the specimens of Schröder-Adams et al. (1990) from eastern Canadian Arctic shelf sediments, but the photographed specimens clearly look like C. distincta and were also assigned as lectotype for this species by Scott et al. (2008). It is noteworthy that the genus Cornuspira does not have an apertural plate, as defined by Schultze (1854), and thus C. distincta should potentially be referred to a different genus.

Glomulina oculus may also express some similarity to juvenile specimens of Miliolinella subrotunda (Montagu), as

Table 1. Measurements of the dimensions of specimens of three, four, and five-chambered *Glomulina oculus* including the range and averages (in brackets) of length and width of the tests and the range of the diameters of the proloculus and the aperture.

Specimen type orfeature	No. of measurements	Length (average)(µm)	Width (average)(μm)	Diameter(µm)
three-chambered	15	134–213 (161)	103–192 (131)	-
four-chambered	6	169–213 (196)	159–175 (168)	-
five-chambered	2	239–244 (242)	150–159 (154)	-
Proloculus	22	<u>-</u> ` ´	<u>-</u> ` ´	53-111
Aperture	7	-	-	24–37

some specimens of *M. subrotunda* do have a large proloculus. However, *M. subrotunda* may be distinguished from *G. oculus* by its quinqueloculine chamber arrangement and a large apertural basal plate, although the latter character can be difficult to identify in juvenile specimens (see Fig. 12.3).

Remarks. Only specimens with a large proloculus were found. Whether this means that only megalospheric (haploid) individuals of Glomulina oculus were found, as recognized for other species with numerous successive asexual cycles (cf., sen Gupta, 1999), or whether there is no difference between haploid and diploid generations is yet uncertain. The fact that some specimens have been found with five chambers, while the majority of specimens have three chambers and the second-most common form has four chambers is somewhat puzzling. One reason may be that the threeand four-chambered individuals are juveniles that because of unfavorable environmental conditions rarely reach maturity (five chambers), but it is also possible that the species is developing towards one that will reproduce in a more juvenile form (netenious species). Retardation of growth may be related to lack of food (cf., Boltovskoy et al. 1991). It is also possible, however, that the normal 'adult' form of the species is in fact three (or four) chambers and that the five-chambered individuals are the ones that, due to harsh living conditions, are not able to reproduce at its regular stage and keep growing for longer time (cf., Boltovskoy et al. 1991). The question on a possible relation between reproduction cycle, ontogeny and ecology was also pointed out by Boltovskoy and Wright (1976) but listed as one of the 'unresolved problems'. Further data on the distribution of the different forms of Glomulina oculus in relation to environmental conditions is needed to help in resolving this issue.

PRESERVATION POTENTIAL AND LIKELIHOOD OF FINDING GLOMULINA OCULUS IN MODERN AND FOSSIL SAMPLES

The preservation potential for Miliolina is generally low because of the high content of Mg in the shells (cf., Brown & Elderfield, 1996; sen Gupta, 1999; Petró et al., 2018). The specimens of Glomulina oculus that we have encountered so far are all very small and thin-shelled. They tend to break very easily, when handled; in particular, the proloculus was broken in many of the specimens (Fig. 8). Even specimens that in light microscope seemed very well-preserved proved, when analyzed in scanning electron microscope, to have been subject to early stages of dissolution and diagenesis, most commonly decomposing the outermost thin organic layer of the test material to reveal the extrados layer of calcareous needle-shaped crystals. Some specimens also showed recrystallization and, likely post-mortem, growth of rhombic calcite crystals in the older parts of the test as well as within the aperture. Also, the thin wall of the proloculus as often broken on one or both sides. However, it is noteworthy that we did indeed find numerous specimens of G. oculus in early Holocene sediments at several meters depth in the cores. Also, the specimens have been subjected to both freeze-drying and oven-drying at low temperatures (25°C) during the laboratory process. This indicates that the preservation potential is not as low as could be assumed from their very thin-walled, fragile porcelaneous tests. Nevertheless, a generally low preservation potential of *G. oculus* might explain why these thin-walled species have not been observed previously, a fact, which is surprising considering its relatively high frequencies in some of our samples. However, it is more likely that it has hitherto been included in counts of other species such as *Cornuspira distincta* and juvenile specimens of *Miliolinella subrotunda*.

CONCLUSIONS

Glomulina oculus n. sp. lives today in the northern Nares Strait and the Petermann Fjord (NW Greenland), as well as off Zachariae Isbrae (NE Greenland) in relation to a stratified water column with chilled and modified Atlantic Water underlying Polar Water. It typically occurs in an environment with marine terminating glaciers and seasonally mobile sea-ice cover that allows episodic marine productivity, and it has an affinity for increased sand content, although further studies are needed to establish its full range of habitats. In sediment cores, Glomulina oculus has been found exclusively in early deglacial glaciomarine sediments of northern Baffin Bay and in similar settings on the NE Greenland shelf. The species has been shown to be reasonably well preserved in both freeze-dried samples and in samples prepared and counted wet, suggesting that the lack of previous registration is presumably not related to a poor preservation state, but rather to its specific environmental requirements and likely also to misidentification in previous studies due to a resemblance to Cornuspira distincta and juvenile specimens of Miliolinella subrotunda.

ACKNOWLEDGMENTS

We are grateful to the captain and crew of *Oden* and the Oregon State University Coring team, for recovering the multicores and to Maziet Cheseby and Laurence Dyke for sampling them on deck. We thank Alan Mix and the scientific party of the 2015 Petermann Glacier Expedition for providing the samples. We thank the Atlantic Geoscience Center, Dartmouth, Canada for access to 2001LSSL-14PC and 2008029-49 and -59P. We are also grateful to the captain, crew, and scientific party of the NorthGreen2017 expedition that helped retrieve cores DA17-NG-ST07-73G and DA17-NG-ST08-90R.

We are furthermore grateful to Electron Microscope (EM) Engineer Ramon Liebrechts from the Interdisciplinary Nanoscience Center (iNANO) at Aarhus University, who provided invaluable help during scanning electron microscope (SEM) photomicrographing. We would also like to thank Professor Kjell Nordberg, University of Gothenburg, Sweden, and Dr. Helena Bergsten for placing their specimens of "Cyclogyrinae" from Bergsten (1994) at our disposal for comparison and to Dr. Teodóra Pados-Dibattista and Joanna M. Davies Aarhus University, for the foraminiferal analyses of the NE Greenland cores. Many thanks to Dr. Kelly Hogan, British Antarctic Survey, for making the map in Figure 1B. We thank Mark Florence of the Smithsonian Natural History Museum for providing the museum numbers for the Holotype and paratypes. We also thank the journal editors and two anonymous reviewers for their comments. Funding for Anne Jennings' research

was provided by National Science Foundation PLR-ANS 1417784, "Collaborative Research: Petermann Gletscher, Greenland - Paleoceanography and Paleoclimatology" and OPP 1804504 "Timing and Paleoceanographic Impacts of the Onset of Arctic-Baffin Bay Throughflow". Marit-Solveig Seidenkrantz was funded by the Independent Research Fund Denmark / Natural Science (G-Ice project grant no 7014-00113B/FNU), and through the NorthGreen2017 expedition grant from the Danish Centre for Marine Research.

REFERENCES

- Aagaard, K., and Coachman, L. K., 1968a, The East Greenland Current north of Denmark Strait, Part I: Arctic, v. 21, p. 181–200.
- Aagaard, K., and Coachman, L. K., 1968b, The East Greenland Current north of Denmark Strait, Part II: Arctic, v. 21, p. 267–290.
- Bergsten, H., 1994, Recent benthic foraminifera of a transect from the North Pole to the Yermak Plateau, eastern central Arctic Ocean: Marine Geology, v. 119, p. 251–267.
- Boltovskoy, E., and Wright, R., 1976, Recent Foraminifera: Dr. W. Junk, The Hague, 515 p.
- Boltovskoy, E., Scott, D. B., and Medioli, F. S., 1991, Morphological variations of benthic foraminiferal tests in response to changes in ecological parameters: A review. Journal of Paleontology, v. 65, p. 175-185.
- Brown, S., and Elderfield, H., 1996, Variations in Mg/Ca and Sr/Ca ratios of planktonic foraminifera caused by postdepositional dissolution: Evidence of shallow Mg-dependent dissolution: Paleoceanography, v. 11, p. 543–551.
- Darling, K. F., Schweizer, M., Knudsen, K. L., Evans, K. M., Bird, C., Roberts, A., Filipsson, H., Kim, H.-J., Gudmundsson, G., Wade, C. M., Sayer, M. D. J., and Austin, W. E. N., 2016: The genetic diversity, phylogeography and morphology of Elphidiidae (Foraminifera) in the Northeast Atlantic: Marine Micropalaeontology, v. 129, p. 1–23.
- Delage, Y., and Herouard, E., 1896, Traité de Zoologie Concrète, Vol 1, La Cellule et les Protozoaires: Schleicher Frères, Paris, 618 p.
- Dunbar, M., 1969, The geophysical position of the North Water: Arctic, v. 22, p. 438–441.
- Ellis, B. F., and Messina, A., 1949 (and update supplements), Catalogue of Foraminifera: American Museum of Natural History and Micropalaeontology Press, New York (ISBN 978-0-913424-34-6), http://wwwmicropress.org/em/about.php (Accessed 22-06-2019).
- Gooday, A. J., and Hughes, J. A., 2002, Foraminifera associated with phytodetritus deposits at a bathyal site in the northern Rockall Trough (NE Atlantic): seasonal contrasts and a comparison of stained and dead assemblages: Marine Micropaleontology, v. 46, p. 83–110.
- Hald, M., and Korsun, S., 1997, Distribution of modern benthic foraminifera from fjords of Svalbard, European Arctic: Journal of Foraminiferal Research, v. 27, p. 101-122.
- Heuzé, C., Wåhlin, A., Johnson, H. L., and Münchow, A., 2017, Pathways of meltwater export from Petermann Glacier, Greenland: Journal of Physical Oceanography, v. 47, p. 405–418.
- Jakobsson, M., Hogan, K. A., Mayer, L. A., Mix, A., Jennings, A., Stoner, J., Eriksson, B., Jerram, K., Mohammad, R., Pearce, C., Reilly, B., and Stranne, C., 2018, The Holocene retreat dynamics and stability of Petermann Glacier in northwest Greenland: Nature Communications, v. 9, https://doi.org/10.1038/s41467-018-04573-2.
- Jennings, A., and Andrews, J., 2019, Petermann Expedition, Oden July 2015, marine core data for mineralogy, foraminifera and particle size, Greenland, 2019: Arctic Data Center, doi: 10.18739/A2MP4VN1H.
- Jennings, A. E., Weiner, N. J., Helgadottir, G., and Andrews, J. T., 2004, Modern foraminiferal faunas of the southwestern to northern Iceland shelf: Oceanographic and environmental controls: Journal of Foraminiferal Research, v. 34, p. 180–207.
- Jennings, A. E., Sheldon, C., Cronin, T. M., Francus, P., Stoner, J., and Andrews. J., 2011, The Holocene history of Nares Strait: Transition from glacial bay to Arctic-Atlantic throughflow: Oceanography, v. 24, p. 26–41.

- Jennings, A. E., Andrews, J. T., Oliver, B., Walczak, M., and Mix, A., 2019, Retreat of the Smith Sound Ice Stream in the Early Holocene: Boreas, v. 48, p. 825-840.
- Jennings, A. E., and Helgadóttir, G., 1994, Foraminiferal assemblages from the fjords and shelf of eastern Greenland: Journal of Foraminiferal Research, v. 24, p. 123–144.
- Kozo, T. L., 1991, The hybrid polynya at the northern end of Nares Strait: Geophysical Research Letters, v. 18, p. 2059–2062.
- Kwok, R., 2005, Variability of Nares Strait ice flux: Geophysical Research Letters, v. 32, doi: 10.1029/2005GL024768.
- Kwok, R., Toudal Pederson, L., Gudmandsen, P., and Pang, S.S., 2010, Large sea ice outflow into the Nares Strait in 2007: Geophysical Research Letters, v. 37, doi: 10.1029/2009GL041872.
- Larsen, N. K., Levy, L. B., Carlson, A. E., Buizert, C., Olsen, J., Strunk, A., Bjørk, A. A., and Skov, D. S., 2018, Instability of the Northeast Greenland Ice Stream over the last 45,000 years. Nature Communications 9, 1872. Doi:10.1038/s41467-018-04312-7.
- Lloyd, J. M., 2006, Modern distribution of benthic foraminifera from Disko Bugt, West Greenland: Journal of Foraminiferal Research, v. 36, p. 315–331.
- Loeblich, A. R., Jr., and Tappan, H., 1994, Foraminifera of the Sahul Shelf and Timor Sea: Cushman Foundation for Foraminiferal Research, Special Publication, No. 31, 661 p.
- Makinson, K., and Anker, P. G., 2014, The BAS ice-shelf hot-water drill: Design, methods and tools: Annals of Glaciology, v. 55, p. 44–52.
- Melling, H., Gratton, Y., and Ingram, G., 2001, Ocean circulation within the North Water polynya of Baffin Bay: Atmosphere-Ocean, v. 39, p. 301–325.
- Millet, F. W., 1898, Report on the Recent foraminifera of the Malay Archipelago collected by Mr. A. Durrand, F. R. M. S., Part III: Journal of the Royal Microscopical Society, p. 607-614.
- Muenchow, A., 2019, Physical ocean property profile from Petermann Fjord, Greenland, surveyed in 2015 by IB/Oden. Arctic Data Center. doi:10.18739/A2XS5JH16.
- Münchow, A., Falkner, K. K., Melling, H., Rabe, B., and Johnson, H. L., 2011, Ocean warming of Nares Strait bottom waters off Northwest Greenland, 2003–2009: Oceanography, v. 24, p. 114–123.
- Münchow, A., Padman, L., Washam, P., and Nicholls, K. W., 2016, The ice shelf of Petermann Gletscher, North Greenland, and its connection to the Arctic and Atlantic Oceans: Oceanography, v. 29, p. 84–95.
- Osterman, L. E., Poore, R. Z., and Foley, K. M., 1999, Distribution of benthic foraminifers (>125 μ m) in the surface sediments of the Arctic Ocean: US Geological Survey Bulletin no. 2164, p. 1–28.
- Parker, J. H., 2017, Ultrastructure of the test wall in modern porcelaneous foraminifera: implication for the classification of the Miliolida: Journal of Foraminiferal Research, v. 47, p. 136-174.
- Petró, S. M., Pivel, M. A. G., and Coimbra, J. C., 2018, Foraminiferal solubility rankings: A contribution to the search for consensus: Journal of Foraminiferal Research, v. 48, p. 301–313.
- Reilly, B. T., Stoner, J. S., Mix, A. C., Walczak, M. H., Jennings, A. E., Jakobsson, M., Dyke, L., Glueder, A., Nicholls, K., Hogan, K. A., Mayer, L. A., Hatfield, R. G., Albert, S, Marcott, S., Fallon, S., and Cheseby, M., 2019, Holocene break-up and reestablishment of the Petermann Ice Tongue, northwest Greenland: Quaternary Science Reviews, v. 218, p. 322-342.
- Rhumbler, L., 1936, Foraminiferen der Kieler Bucht, gesammelt durch A. Remane, Teil II Ammodisculinidae bis einschluss Textularinidae: Kieler Meeresforschungen, v.1, p. 179–242.
- Ryan, P. A., and Münchow, A., 2017, Sea ice draft observations in Nares Strait from 2003 to 2012: Journal of Geophysical Research, Oceans, v. 122, p. 3057–3080.
- Saidova, K. M., 1981, On an up-to-date system of supraspecific taxonomy of Cenozoic benthonic foraminifera. Moscov: Institut Okeanologi P. P. Shirshova, Akadamia Nauk, SSSR. 73 p (in Russian).
- Samelson, R. M., Agnew, T., Melling, H., and Münchow, A., 2006, Evidence for atmospheric control of sea-ice motion through Nares Strait: Geophysical Research Letters, v. 33, L02506, doi: 10.1029/2005GL025016.

- Schröder-Adams, C. J., Cole, F. E., Medioli, F. S., Mudie, P. J., Scott,
 D. B., and Dobbin, L., 1990, Recent Arctic shelf foraminifera:
 Seasonally ice covered vs. perennial ice covered areas: Journal of Foraminiferal Research, v. 20, p. 8–36.
- Schultze, M. S., 1854, Über den Organismus der Polythalamien (Foraminiferen), nebst Bemerkungen über die Rhizopoden im Algemeinen: Wilhelm Engelmann, Leipzig, 68 p.
- Scott, D. B., Schell, T., Rochon, A., and Blasco, S., 2008, Modern benthic foraminifera in the surface sediments of the Beaufort shelf, slope and Mackenzie Trough, Beaufort Sea, Canada: Taxonomy and summary of surficial distribution: Journal of Foraminiferal Research, v. 38, p. 228–250.
- Seidenkrantz, M.-S., 1995, Cassidulina teretis Tappan and Cassidulina neoteretis new species (Foraminifera): Stratigraphic markers for deep sea and outer shelf areas: Journal of Micropalaeontology, v. 14, p. 145–157.
- sen Gupta, B. K., 1999, Modern Foraminifera: Kluwer, Dordrecht, The Netherlands, 371 p.

- Tang, C., Ross, C., Yao, T., Petrie, B., Detracey, B., and Dunlap, E., 2004, The circulation, water masses and sea-ice of Baffin Bay: Progress in Oceanography, v. 63, p. 183–228.
- Washam, P., Münchow, A., and Nicholls, K. W., 2018, A decade of ocean changes impacting the ice shelf of Petermann Gletscher, Greenland: Journal of Physical Oceanography, v. 48, p. 2477–2493.
- Washam, P., Nicholls, P. W., Münchow, A., and Padman, L., 2019, Summer surface melt thins Petermann Gletscher Ice Shelf by enhancing channelized basal melt: Journal of Glaciology, doi: 10.1017/jog.2019.43.
- Wollenburg, J. E., and Mackensen, A., 1998, Living benthic foraminifera from the central Arctic Ocean: Faunal composition, standing stock and diversity: Marine Micropaleontology, v. 34, p. 153–185.

Received 9 August 2019 Accepted 15 February 2020

